Femtomole Detection Of Proteins Using A Label-Free Nanostructured Porous Silicon Interferometer For Perspective Ultra-Sensitive Biosensing

*Stefano Mariani, Lucanos Marsilio Strambini, Giuseppe Barillaro**

Dipartimento di Ingegneria dell'Informazione, Università di Pisa, via G. Caruso 16, 56122 Pisa, Italy

**g.barillaro@iet.unipi.it*

Abstract

Nanostructured porous silicon (PS) is a promising material for the label-free optical detection of biomolecules, but it currently suffers of limited clinical diagnostic applications due to insufficient sensitivity. In this regard, here we introduce an ultrasensitive and robust signal processing strategy that relies on the calculation of the average value over wavelength, namely IAW, of spectral interferograms attained on a PS interferometer by subtraction (wavelength by wavelength) of reflection spectra acquired after adsorption of biomolecules inside the nanopores from a reference spectrum recorded in acetate buffer. As a model we have chosen Bovine Serum Albumin (BSA) unspecific adsorption, which has been often employed in the literature for proof-of-concept studies of perspective biosensing applications.

The proposed IAW signal processing strategy enables reliable detection of BSA at concentrations in the range 150 pM - 15 μM (down to 3 orders of magnitude lower than those targeted in the current literature) using a PS interferometer operating in label-free mode without any amplification strategies, with good sample-to-sample reproducibility over the whole range of tested concentrations (%CV= 16% over 5 replicates) and good signal-to-noise ratio (S/N ~ 4.6) also at the lowest tested concentration (150 pM). A detection limit (DL) of 20 pM (20 femtomole, 1 ml) is

estimated from the sigmoidal function best fitting (R^2=0.989) IAW experimental data over the whole range of tested concentrations. This is the lowest DL that has been reported in the literature since the seminal paper of Sailor and coworkers (1997) on the use of PS interferometer for biosensing, and lowers of 4 orders of magnitude the best DL attained with label-free PS interferometers using conventional effective optical thickness (EOT) calculation obtained by reflective interferometric Fourier transform spectroscopy. Accordingly, the IAW signal processing strategy envisage bringing PS optical transduction at the forefront of ultrasensitive label-free biosensing, especially for point-of-care clinical analysis where low analyte concentrations have to be detected in small amount of real biological samples.

Keywords: nanostructured porous silicon, interferometer, ultrasensitive detection, femtomole, label-free, protein

INTRODUCTION

According to recent surveys, the global biosensor market is expected to grow up to about USD 21 billion by 2020, with increasing demand for sensitive, specific, and real-time devices in healthcare and point-of-care fields.[1] Among others (i.e. electrochemical, piezoelectric),[2] optical transduction has been thoroughly investigated over the last two decades for its intrinsic high sensitivity both in fluorescence and label-free (i.e. based on detection of refractive index –RI– variation) modes.[3] Porous silicon (PS) is an increasingly exploited nanostructured material for the preparation of interferometric label-free (bio)sensors thanks to its high degree of biocompatibility, high versatility, easy fabrication, and low cost.[4-8] PS (bio)sensors are currently used for different applications ranging from environmental control to food monitoring, from clinical diagnostics to point of care analysis.[5-7]

The first demonstration of optical biosensing with PS was given in 1997 by Sailor and coworkers both in antibodies and in DNA affinity detection, for which pico- and femtomolar detection limit

(DL) were achieved using an optimized assay design in terms of immobilization chemistry.[9] Following that seminal research, an intense effort has been paid to the use PS optical interferometric biosensors both in DNA affinity detection[10,11] and in protein detection.[12-19] As to protein detection, immobilization steps, signal processing, and PS preparation have been firstly optimized using suitable models, e.g. either studying reversible binding of IgG on protein A coated mono-layered surfaces[12] (also using IgG derived from different animal species on protein A,[13] with IgG on protein A using self-compensating double-layer,[14] with IgG on protein A using serum or whole blood by exploiting intrinsic PS size-exclusion filtering[15]) or investigating streptavidin immobilization within different pore size biotinylated surfaces[16] and using short peptides as linker for biotin;[17] afterward, specific assays for detection of molecules of clinical interest have been then developed, e.g. for either small peptide his-tag detection with aptamer[18] or protein subunit B of cholera toxin detection by hybrid lipid bi-layered membrane bio-mimetic PS scaffold.[19] Further, PS interferometric biosensors have been also reported for the detection of small organic molecules of clinical or environmental interest, e.g. glutamine,[20] opiates,[21,22] glucose,[23] and warfare toxic compound, e.g. fluorophosphates using catalytic gas chemosensor.[24] Finally, PS interferometers have been employed for studying enzymatic activity of protease[25-28] and glutathione-Stransferase,[29] and, more recently, for monitoring single cell activity,[30] e.g. by capturing bacteriausing IgG[31] or by monitoring bacteria lysates using peptidomimetic antimicrobial compounds.[32]

In spite of such an intensive and successful use of PS interferometer for (bio)sensing, in 2015 Segal and coworkers have emphasized how PS biosensors still suffer of limited real clinical diagnostic applications due to insufficient sensitivity caused by mass-limited diffusion of target molecules inside the nanopores.[33] As a matter of fact, none reached detection limits comparable to those reported by Sailor and coworkers in 1997,[5] by direct, label-free, optical detection using PS, the best reported one being currently in the micromolar level both for DNA [11,33] and proteins. [14,18]

This fact has steered researchers toward signal amplification strategies[13,33,35-38] able to push detection limit of PS biosensors down to that of others high sensitivity label-free optical techniques,

e.g. Surface Plasmon Resonance (SPR) with detection limits in (and below) the nanomolar level.[34] As to label-free amplification strategies, in 2007, Sailor and coworkers by-passed the problem of biomolecule diffusion inside PS by continuously circulating 4mL of IgG solution on a protein A covered nanopore surface, thus pushing the detection limit down to 50 nM.[13] More recently, Segal and coworkers proposed a novel microfluidic platform that exploits electrokinetic focusing to enhance DNA diffusion and hybridization inside PS, thus reaching a detection limit of 1 nM.[33] Besides, non label-free amplification strategies have been also reported. For instance, in 2011, Voelcker and coworkers reported enzymatic amplification by horseradish peroxidase (HRP) mediated oxidation of TMB on antibody-functionalized PS for human IgG detection with detection limit down to 0.2 μg/ml.[35] In 2012, the same group reported polymerization-amplified detection of DNA for single nucleotide mismatch detection.[36] In 2014, Voelcker and coworkers exploited fluorescence-enhanced protein detection using a fluorogenic MMP (Matrix Metalloproteinase) peptide immobilized on the nanopore surface of a resonant microcavity to push the detection limit of MMP-1down to 7.5×10^{-19} M.[37] In 2015, Gooding and coworkers employed proteolytic action against peptides dispersed in a synthetic polymeric substrates in nanopores for the detection of MMP9 with detection limit of 0.37 pM.[38]

This overview clearly highlights the need for improving analytical performance (higher sensitivity and lower detection limit) of PS interferometers for optical affinity biosensors, which perfectly fits the research reported in this work concerning direct, label-free, and ultrasensitive optical detection of proteins using PS. As a model system we have used Bovine Serum Albumin (BSA) unspecific adsorption inside the inner PS surface, a cheap and effective model often exploited in literature for proof of concept demonstrations of perspective biosensing applications.[39,40] A simple, sensitive, and robust signal processing strategy based on the calculation of the average value spectral interferograms over wavelength, namely IAW, is developed. Interferograms are obtained by subtracting (wavelength by wavelength) reflection spectra acquired on a PS interferometer upon BSA adsorption on the nanopore surface from a reference spectrum recorded in acetate buffer. The

IAW signal processing strategy allows to reliably detect BSA at concentrations ranging from 150 pM to 15 μM (down to 3 orders of magnitude lower than those detected in the state of the art literature) using a PS interferometer operating in label-free mode without any amplification strategies. A good sample-to-sample reproducibility is obtained over the whole range of tested concentrations (%CV= 16% over 5 replicates), with a good S/N (~ 4.6) already at the lowest concentration (150 pM). A sigmoidal behavior encompasses the whole range of tested concentrations (R^2=0.989) and yields a detection limit (DL) of 20 pM (20 femtomole, 1 ml). This is the lowest detection limit that has been reported in the literature on PS interferometer for biosensing applications since the seminal paper of Sailor and coworkers (1997),[9] and lowers DL of PS interferometers in biosensing of 4 orders of magnitude with respect to the best DL obtained using conventional effective optical thickness (EOT) calculation through reflective interferometric Fourier transform spectroscopy. Accordingly, the IAW processing strategy envisages using PS interferometers in point of care applications for direct and effective label-free targeting of low analyte concentration in a small amount of real samples (e.g. in-trace miRNA biomarkers directly from biological samples in "liquid biopsy" for tumor diagnosis).[41]

MATERIALS AND METHODS

Materials and Chemicals

Silicon wafer boron doped, <100> oriented, resistivity of 0.8-1.2 mΩ-cm, are purchased from Siltronix, Inc.(France). Aqueous hydrofluoric acid (HF 48%), absolute ethanol (99.8%), sodium hydroxide (NaOH >98%), isopropyl alcohol (99.7%), anhydrous pentane (98%), sodium chloride (NaCl 99%), acetic acid (CH_3COOH 99.5%), sodium acetate (CH_3COONa 99%), and bovine serum albumin (BSA, ≥98%, pI = 4.7, MW = 66,430 Da) are purchased from Sigma Aldrich (Germany). Aqueous acetate buffer is prepared dissolving 10.0 mM CH_3COONa/CH_3COOH and 100 mM NaCl in deionized water (DIW), adjusted to pH = 4.70, filtered using syringe filters (Minisart® NML Syringe Filters 1.20 μm), and used both as a running buffer and as a solvent to solubilize BSA.

Preparation and oxidation of PS samples

Porous silicon samples are prepared by a two-steps anodic etching of highly doped *p*-type silicon using a solution of HF(48%):EtOH, 3:1 v/v. Caution: HF is a highly corrosive acid, and it has to be handled with extreme care under safety work conditions! Silicon samples (area of 0.567 cm^2) are placed in a two-electrodes Teflon cell equipped with an aluminum flat anode and a platinum wire cathode and driven by a Keithley 2602A SourceMeter. A first PS sacrificial layer is prepared at 200 mA/cm^2 for 30 s and dissolved in a NaOH(1M):EtOH, 9:1 v/v solution to avoid the presence of a top parasitic layer restricting effective diffusion of large molecules, e.g. proteins, in the PS layer underneath.[8] After NaOH dissolution, silicon samples are thoroughly rinsed with ethanol and dried under nitrogen flow. A second PS sensing layer is prepared on NaOH-treated silicon samples by anodic etching at 400 mA/cm^2 for 20 s. PS samples are then rinsed with 2-propanol and pentane, and dried under nitrogen flow to obtain a crack-free PS layer. Eventually, PS samples are thermally oxidized in a muffle furnace (ZB 1, ASAL, Italy) at 750°C for 1h (ramp-up/ramp-down 12°C/min) in room atmosphere.

Morphological and optical characterization of PS samples

Top view and cross-section of as-prepared PS samples are investigated using a Scanning Electron Microscope (SEM, JEOL JSM-6390, ITALY) at an accelerating voltage of 5 kV so as to infer on both size and length of pores, respectively. Porosity is numerically estimated by fitting experimental reflection spectra of as-prepared PS samples with a home-made software developed in MatLab (MathWorks®, USA).[42]

Both as-prepared and thermally-oxidized PS samples are optically characterized in air in the wavelength range 400-1000 nm using a fiber-optic setup consisting of a halogen lamp source (HL-2000), a bifurcated fiber-optic probe (QR200-7-VIS-BX), and a UV-VIS spectrometer (USB2000-VIS-NIR-ES) purchased from Ocean Optics (USA). Light exiting from the halogen lamp source is

fed through one arm of the bifurcated fiber-optic probe orthogonally onto the PS surface and the reflected light is collected through the other arm of the bifurcated fiber-optic probe into a UV-VIS spectrometer that yields the reflection spectra.

Acquisition parameters of reflection spectra are: integration time of 2 ms, average scan number 5, boxcar width 5, with spectrometer working in photon counts mode.

Experimental setup and infiltration protocol for BSA

A flow-cell system integrated with the fiber-optic setup previously described is used for the optical characterization of PS samples in the presence of acetate buffer at different BSA concentrations. The PS sample is secured into a home-made Plexiglas flow-cell with volume of 100 μL. The flow-cell is connected to a Nexus 3000 (Chemyx Inc., USA) syringe pump working in withdraw mode, through which solutions under test are injected in the flow-cell at a flow-rate of 25 μL/min. Acetate buffer is firstly injected for a warm-up time of 60 minutes before reflection spectra are recorded, which ensures both fluidic and thermal transient are fully over. After the warm-up time is elapsed a reference reflection spectrum in acetate buffer is acquired. Acetate buffer is further flushed for 50 minutes in the flow-cell, and then a novel reflection spectrum is acquired before starting injecting BSA solutions and used for both blank signal and instrumental noise evaluation. BSA solutions with concentration in the range 150 pM-15 μM (150 femtomoles-15 nanomoles, 1 mL) are then injected for 40 min (1 mL total volume) for each concentration value using acetate buffer as a carrier, starting with the lower concentration value and acquiring reflection spectra every 10 minutes since the injection has started. A rinse step in acetate buffer of 10 min follows injection of each BSA concentration value so as to empty the nanopores from BSA not adsorbed on the pore surface, then a reflection spectrum is acquired at the end of the rinse step before injection of the next BSA concentration value. Analytical quantification of BSA adsorption in the PS layer at each tested concentration is carried out through analysis of experimental reflection spectra according to the signal processing strategy described in the Results and Discussion section.

Evaluation of BSA adsorption kinetics in the inner PS surface is carried out for some specific concentrations (namely, 15 μM) according to the protocol above described, though reflection spectra are acquired every single minute.

Acquisition parameters of reflection spectra are: integration time of 2 ms, average scan number 5, boxcar width 5, with spectrometer working in normalized reflectivity mode.

Effective optical thickness calculation by FFT

Effective Optical Thickness (EOT), namely $2nL$ with n effective refractive index and L thickness of the PS layer, respectively, is estimated by reflective interferometric Fourier transform spectroscopy using a home-made software developed in MatLab (MathWorks®, USA). The wavelength axis of each PS reflection spectrum is firstly inverted (x-axis changed from wavelength to 1/wavelength) to get a wavenumber axis, then a cubic-spline interpolation is applied to reflection data so as to have a dataset (reflection, wavenumber) spaced evenly (sample-to-sample distance 8.57×10^{-7} nm^{-1}). A Hanning window is applied to the reflection spectrum and it is zero-padded to a power of two, specifically 2^{24}. Eventually, the FFT algorithm is applied to the zero-padded reflection spectrum, which yields both Fourier transform amplitude and phase (y-axis in the Fourier transform domain) as a function of length, i.e. 1/wavenumber (x-axis in the Fourier transform domain), with spatial resolution of about 0.07 nm. The EOT value corresponds to the 1/wavenumber axis (x-axis) value in the Fourier transform domain for which the main peak in the Fourier Trasform amplitude (y-axis) occurs.

RESULTS AND DISCUSSIONS

Porous silicon preparation and oxidation

PS samples, produced by anodic etching in ethanoic HF solution of highly doped *p*-type silicon, are at first morphologically and optically characterized. In Fig. 1a and 1b SEM images of typical cross-section and planar views of freshly etched PS samples are reported. From SEM images a columnar-

like structure is apparent (Fig. 1a) with pores sizes between 50 and 80 nm (Fig. 1b), which are large enough to allow effective infiltration of proteins with characteristic dimensions of a few nm, such as BSA (about 4.0 x 4.0 x 12 nm^3).[43] PS thickness, evaluated by SEM measurements and averaged over six samples, is 2.95 ± 0.14 µm (%CV ~ 4.7%). The PS thickness is chosen according to former works on BSA adsorption in PS using a flow-over approach (~3-5 μm)[39,40]. Porosity (%), numerically estimated by a computational method based on the analysis of reflection spectrum[42] and averaged over six samples, is 75.5 ± 0.4% (%CV ~ 5.3%). Specific surface, numerically estimated by geometrical approximation of pores as ideal columnar structures with height of 2.95 µm (average PS thickness) and diameter of 65 nm (average pore size), is 48 m^2/cm^3. Reliability and reproducibility of the PS production process is good, as testified by low %CV values of both porosity and thickness. Optical characterization of as-prepared PS samples is performed by UV-VIS reflectance spectroscopy in the wavelength range 400-1000 nm. A typical reflectance spectrum of as-prepared PS samples recorded in air is shown in Fig. 1c (black trace).

As-prepared PS samples are thermally oxidized in a muffle furnace at 750°C for 1h and then cooled down to room temperature (18 °C). A typical reflectance spectrum of oxidized PS samples recorded in air is shown in Fig. 1c (red trace). Oxidation of the PS silicon skeleton is confirmed by contact angle measurements using deionized water (DIW), which highlight a significant decrease of the contact angle upon oxidation, from ~110° of freshly etched PS to ~13.5° of oxidized PS (Fig. 1d). PS oxidation is also confirmed by FFT analysis of the reflection spectra acquired before and after thermal treatment, which shows a typical blue-shift of the EOT value after oxidation, from about 9247 nm of as-prepared PS to about 7763 nm of oxidized PS (Supporting Information). PS surface oxidation has a twofold aim: controlling passivation of nanopore surface so as to avoid uncontrolled oxidation over time; increasing hydrophilicity so as to improve infiltration in the nanopores of acetate buffer and promote BSA adsorption on the inner nanopore surface.

BSA infiltration and signal processing strategy

BSA solutions are prepared in acetate buffer (pH = pI_{BSA} = 4.7) at concentrations ranging from 150 pM to 15 μM (150 femtomoles - 15 nanomoles, 1.0 mL). The use of acetate buffer (10.0 mM CH_3COONa/CH_3COOH and 100 mM NaCl) allows maximizing protein diffusion and adsorption in the nanopores, occurring when BSA is both globally neutral (condition reached with pH = pI_{BSA}) and deeply shielded by a high ionic strength (condition reached with 100 mM NaCl).[40] In fact, by minimizing ionic protein-protein repulsions outside the nanopores, BSA diffusion inside the nanopores is encouraged and its adsorption on the nanostrucured surface is, in turn, enhanced.[40] Both acetate buffer and BSA solutions are injected into a flow-cell containing the PS sample at a rate of 25 μL/min and reflection spectra are acquired according to the protocol detailed in Materials and Methods.

The proposed analytical signal processing strategy for direct label-free BSA detection using a PS interferometer relies on the calculation of the average value over wavelength of spectral interferograms, namely IAW. For each tested BSA concentration, interferograms are calculated by subtraction of the reflection spectrum acquired after each BSA injection from a reference reflection spectrum acquired in acetate buffer. All interferograms are referred to a reference interferogram calculated for acetate buffer before starting any BSA injection. The details of the IAW signal processing strategy are here in the following given and discussed with respect to the highest BSA concentration tested in this work (i.e. 15 μM, 15 nanomoles in 1 mL), also with reference to Fig. 2 that highlights the outcomes of the main processing steps.

The first step deals with the calculation of the interferograms from reflection spectra recorded in acetate buffer and after infiltration of PS with any tested BSA concentration. Reflection spectra are all acquired in acetate buffer, either before starting BSA injection or after injection of each BSA concentration value. In Fig. 2a as-acquired reflection spectra in acetate buffer both before starting BSA injection (black trace) and after injection of 15 μM BSA (red trace) are shown. A slight but clear change in the reflection spectrum is observable, which is theoretically explained in terms of intensity, phase, and frequency changes of the Fabry-Perot fringes that are originated by

constructive-destructive interference of light within the PS layer. Such a change of the reflection spectrum is ascribable to BSA bioaccumulation on the nanopore surface, being the contribution of BSA molecules dispersed in the buffer negligible. In fact, according to Pacholski et al., 2005,[39] BSA refractive index at concentration of 15 μM (which is the highest concentration tested in this work) in buffer with pH=4 is 1.3365 and it is indistinguishable from refractive index of pure buffer. In addition, reflection spectra are acquired after a 10 minute rinsing step following BSA injection, which ensures BSA molecules dispersed in acetate buffer are further diluted, at least, if not fully removed. Reflection spectra are normalized with respect to a reference mirror before calculation of the interferograms. Although this is not a mandatory operation, it allows compensating (partially) for non-idealities of the spectrometer (e.g. reduction of the sensitivity at the edge of the wavelength range under investigation). Interferograms are then calculated by subtraction of reflection intensity (wavelength by wavelength) of the normalized reflection spectrum acquired for each BSA concentration from a normalized reference reflection spectrum acquired in acetate buffer at the end of the warm-up time. Subtraction of reflection spectra was for the first time reported by Sailor and coworkers to visually highlight changes in the reflection spectrum before and after binding of specific analytes in a bio-affinity assay,[9] but to our best knowledge no report on the analytical validation and application of a signal processing strategy based on use of interferograms for (even perspective) quantitative biosensing applications has been published. All the interferograms are limited in the wavelength region 500-800 nm, where the spectrometer used in this work has higher signal-to-noise ratio. Fig. 2b reports a typical interferogram obtained for BSA 15 μM (red trace), which appears as a pseudo-periodic signal with peaks and valleys originated by the mismatch of the reflection spectrum after BSA adsorption in the nanopores with respect to the reference reflection spectrum in acetate buffer. A reference interferogram is calculated for acetate buffer by subtraction of the normalized reflection spectrum acquired in acetate buffer right before injecting the first BSA concentration (i.e. 50 minutes after the warm-up time is elapsed) from the normalized reference reflection spectrum. The reference interferogram is used to calculate the instrumental noise floor to

which BSA interferograms are referred to. Fig. 2b shows the typical reference interferogram of acetate buffer (black trace), which appears as noise spanned over the whole wavelength range under condideration. From Fig. 2b it is clear that the interferogram of BSA 15 μM is significantly higher than that of the acetate buffer, thus highlighting that 15 μM of BSA are effectively discerned using a PS interferometer operating in direct label-free mode.

The second step deals with the removal of the average value of interferograms calculated for any BSA concentration, so as to reduce possible artifacts on the spectral reflection intensity induced by unwanted (though unavoidable) BSA adsorption on top of the PS layer, as pointed out by Pacholski et al.,[44] and/or on the flow-cell quartz window through which optical measurements are carried out. Artifacts on the reflection intensity might significantly affect PS biosensors especially in terms of reproducibility from samples to samples at the higher analyte concentrations, as it is here demonstrated in the next paragraph "*Calibration curve and analytical performance*". Fig. 2c shows the two interferograms of Fig. 2b after the average values are removed, thus yielding interferograms (almost) symmetrical with respect the x-axis.

The final step deals with the calculation of the output signal from interferograms obtained for any BSA concentration, namely Interferogram Average over Wavelength (IAW), which is performed by applying the absolute value function to interferograms resulting from step 2 and then calculating the average value of the subsequent interferograms over the whole spectral range of interest (500-800 nm). Application of the absolute value function allows obtaining a full positive interferogram whose IAW value differs from zero and is correlated to the information carried out from the interferogram itself, which increases as the BSA concentration increases. Fig. 2d shows the interferograms obtained for BSA 15 μM and acetate buffer after application of the absolute value function to data of Fig. 2c. Taking the average value of interferograms over wavelength allows to significantly increase the output signal robustness, e.g. with respect to only take the maximum value of interferogram peaks at either single or multiple specific wavelengths. In fact, while the latter is not accurate being strongly dependent on the noise level around the specific peak taken into account

(see noisy peaks in Fig. 3d), the former is considerably more accurate being the effect of noise reduced from the definite integral operation (see output signals in Fig. S1). Fig. S1a and S1b show the typical interferogram integral value (i.e. definite integral of interferogram amplitude over wavelength in the wavelength range [500 - λ^*] nm, with λ^* spanning over the whole range under investigation 500-800 nm) and average value (i.e. ratio between the integral value and the width (λ^*-500) nm of the wavelength interval under consideration), respectively, for the full set of BSA concentrations tested, for one of the PS samples of this work. Independently of the BSA concentration value, the integral value (Fig. S1a) increases almost linearly as the wavelength integration interval increases, whereas the average value (Fig. S1b) initially increases then tends to quickly stabilize to its final value, namely IAW, after a wavelength integration interval of about 100 nm. Remarkably, both integral and average values allow discriminating between different BSA concentrations when the wavelength integration interval increases over 100 nm. The IAW values for BSA 15 μM (1.0 mg/mL) and acetate buffer (blank signal) calculated in the range 500-800 nm over five replicates are 0.595 ± 0.080 (a.u.) and 0.067 ± 0.008 (a.u., IAW_0), respectively, which yield a net differential IAW signal of 0.528 ± 0.080 (a.u.). The standard deviation of the acetate buffer IAW_0 value, namely σ_{IAW0}= 0.008 (a.u.), allows estimating the sample-to-sample experimental noise floor of our PS interferometer in acetate buffer, which is about 74 times smaller than the IAW value for BSA 15 μM.

Fig. 3a shows the IAW–IAW_0 signal *versus* time at sampling rate of 1 minute for the PS interferometer of this work in acetate buffer before injecting BSA (minutes 0-10), during injection of BSA 15 μM (minutes 10-50), and in acetate buffer after BSA injection (rinsing step, minutes 50-60). From Fig. 3a it can be assessed that BSA rapidly diffuses inside the nanopores and significantly adsorbs on their surface in about 5 minutes, then adsorption saturates during the following 30 minutes. This saturation trends well agrees with kinetics models reported in literature for protein adsorption on PS oxidized surface.[45] Fig. 3a allows estimating the experimental noise floor over time of our PS interferometer for a given sample from the standard deviation of the IAW_0

value in acetate buffer (baseline) before (from 0 to 10 min) and after (from 50 to 60 min) injection of BSA. Remarkably, the noise floor over time for a given sample is 0.005 (a.u.), which is in good agreement with the sample-to-sample noise floor (σ_{IAW0} = 0.008 a.u., previously reported).

Calibration curve and analytical performance

Fig. 3b shows the calibration curve in semi-log scale (linear scale in inset) for BSA unspecific adsorption obtained with the PS interferometer of this work at concentrations in the range 150 pM-15 μM. The IAW values calculated for each BSA concentration are subtracted from the IAW_0 blank value in acetate. A typical sigmoidal trend is observed and a significant signal ($IAW–IAW_0$ = 0.037 ± 0.012 a.u.) is recorded also at the lowest tested concentration (150 pM), with a good signal-to-noise ratio (S/N~ 4.6), if compared to the noise floor σ_{IAW0} = 0.008 a.u., and a satisfactory reproducibility (%CV = 32%), especially if one considers the very low level of concentration tested and detected. The calibration curve is best-fitted (R^2 = 0.989) by the sigmoidal function in Eq. 1:

$$IAW - IAW_0 = A - (A - B)e^{-(kC)^d} \quad (1)$$

being C the BSA concentration, and A = 0.516, B = 0.024, k = 2.617, and d = 0.558 fitting parameters. From Eq. 1 it is possible to extrapolate the DL for the PS interferometer of this work, which is by definition the concentration value for which the signal-to-noise ratio is 3.3.[46] This is achieved when $IAW–IAW_0 = 3.3\sigma_{IAW0}$ = 0.026 (shown in Fig. 3b as a gray area) and corresponds to a concentration of 20 pM (i.e. 20 femtomoles, 1 mL). In addition, the proposed signal processing strategy proves to be quite robust, with satisfactory reproducibility (over 5 replicates) in terms of averaged %CV= 16% over the whole range of concentrations tested, especially if compared with the standard analysis performed by EOT calculation through conventional FFT analysis of reflection spectra (see next paragraph "*Conventional analysis by EOT calculation"*).

Fig. S2 shows the calibration curve obtained by applying the IAW processing strategy *without* removal of the average value from interferograms (step 2 of the analytical procedure) to the same set of reflection spectra used in Fig. 3b. By comparison of the two calibration curves obtained with

and without average value removal from interferograms a larger data dispersion is evident for the latter (%CV = 34%) with respect to the former (%CV = 16%), which yields a worse sample-to-sample reproducibility. It is interesting to note that IAW_0 values in acetate buffer calculated with and without removal of the average values from interferograms do not show any differences, being 0.067±0.008 in both cases, thus experimentally corroborating that unwanted adsorption of BSA on top of the PS interferometer and/or on the flow-cell window affects measurement reproducibility.

Conventional analysis by EOT calculation

As a benchmark, we performed conventional FFT analysis on the same set of reflection spectra used in Fig. 3b for the IAW analysis, so as to compare EOT changes resulting from BSA adsorption on the nanopore surface with IAW changes. Fig. S3a reports FFT amplitude spectra typical of as-made and oxidized PS samples in air, as well as of oxidized PS samples both in pure acetate buffer and in acetate buffer after injection of BSA 15 μM. A change in the EOT value of about 30 nm after injection of BSA 15 μM, with respect to pure acetate buffer, is observed (Fig. S3b). This change is compatible with former reports on the detection of BSA 15 μM (1.0 mg/ml) where changes in EOT of about 90 nm were recorded in similar conditions (pH=4) using a double-layered PS interferometer, where the PS layer in which BSA was adsorbed had comparable thickness (2.9 um) but higher porosity (85%) than that used in this work.[39] We argue that differences in both PS layer porosity and injected BSA masses between this work and reference[39] are compatible with the smaller EOT change recorded for BSA 15 μM. In fact, here we infiltrate 1 mg/ml of BSA for 40 min at 25 μL/min, which corresponds to 1 mg of BSA dissolved in 1 mL of acetate buffer; in reference[39] authors infiltrate 1.0 mg/ml of BSA for 20 min at 0.5 ml/min, which corresponds to 10 mg of BSA dissolved in 1 mL of acetate buffer, that is a BSA mass 10-fold higher than that used in this work.

Figure S3c shows the calibration curve over the whole range of tested BSA concentrations obtained using EOT values (calculated over 5 replicates on the same reflection spectrum dataset used for the

IAW analysis) as output signal. The EOT values calculated for each BSA concentration are subtracted from the EOT_0 blank value in acetate buffer. The limit of detection achievable with FFT analysis is estimated as the BSA concentration for which $EOT\text{-}EOT_0 = 3.3\sigma_{EOT0} = 17.1$ nm (upper boundary of the gray area in Fig. S3c), being $\sigma_{EOT0} = 5.17$ nm the standard deviation of EOT_0. It is apparent that conventional FFT analysis does not allow to reliably discriminate among the different BSA concentrations used in this work (average %CV over the whole concentration range 129%). Particularly, the BSA concentrations in the range 150 pM – 150 nM are below the detection limit (within the gray area), whereas the two BSA concentrations at 1.5 and 15 μM lie just close to the detection limit (boundary of the gray area). This is in agreement with the current literature on PS biosensors for which the micromolar level is only targeted through the use of signal amplification strategies that allow to increase EOT changes upon biomolecule binding at the nanopore surface and to yield, in turn, the FFT signal processing strategy more effective and reliable both for in-sample and for sample-to sample analyses.

CONCLUSIONS

In this work we prove that nanostructured PS interferometer can be effectively exploited for ultrasensitive and label-free detection of biomolecules without need for time-/reagent-consuming (either ex-ante or ex-post) signal amplification strategies used to overcome insufficient sensitivity of PS for perspective clinical applications.[33] As a benchmark we target unspecific adsorption of BSA into oxidized PS, being this a fast, cheap, and reliable model often exploited in literature for proof-of-concept demonstrations of perspective biosensing.[39, 40]

BSA concentrations in the range 150 pM – 15 μM (150 femtomoles – 15 nanomoles) are successfully monitored with good sample-to-sample reproducibility (%CV= 16% over 5 replicates) and good signal-to-noise ratio (S/N ~ 4.6 for BSA 150 pM). A sigmoidal trend encompassing the whole concentration range is recorded ($R^2 = 0.989$) that yields a DL = 20 pM (20 femtomole, 1 ml). This is the lowest DL reported in the literature since the 1997 seminal paper of Sailor and

coworkers, and envisages the possibility of decreasing detection limit of PS biosensors of orders of magnitude compared to current literature.

To achieve such remarkable analytical performance, we introduce a novel, simple, effective, and reliable signal processing strategy that is based on the calculation of the average value over wavelength of spectral interferograms, namely IAW, to be used as output signal. Interferograms are obtained by subtracting reflection spectra acquired on PS after adsorption of BSA from a reference reflection spectrum acquired in acetate buffer. The IAW output signal allows achieving higher reproducibility (in terms of both in-sample and sample-to-sample reproducibility) and lower detection limit (in terms of minimum detectable concentration over the noise floor) with respect to the EOT output signal obtained by conventional FFT analysis. In fact, comparing IAW and EOT signals arising from the analysis of the same set of reflection spectra, it is apparent that whereas the IAW signal allows to clearly discriminate BSA 150 pM, the EOT signal does not allow to effectively discriminate BSA concentrations underneath the micromolar level.

Concluding, the IAW analytical signal processing strategy proposed in this work allows to better exploit, with respect to conventional reflective interferometric Fourier transform spectroscopy, the potential of PS interferometer for the detection of a specific analyte at low concentration and in a small amount of fluid, both of which act as a bottleneck in point-of-care tests of clinical diagnosis medical relevance.

Author information

Corresponding Author

*Phone: 050 2217601. E-mail: *g.barillaro@iet.unipi.it.*

Notes

The authors declare no competing financial interest.

Acknowledgments

This research was funded by the Italian Minister for University and Research (MIUR) Futuro in Ricerca (FIR) programme, GrantNo. RBFR122KL1 (SENS4BIO).

Supporting Information

Additional figures aimed at better clarifying peculiar aspects of the proposed IAW signal processing strategy, also with respect to the conventional EOT signal processing strategy are provided in Supporting Information.

Reference

(1) www.grandviewresearch.com/press-release/global-biosensors-market. Accessed 15/12/2015.

(2) Turner, A. P. F. *Chem. Soc. Rev.* **2013**, *42 (8)*, 3184–3196.

(3) Fan, X.; White, I. M.; Shopova, S. I.; Zhu, H.; Suter, J. D.; Sun, Y. *Anal. Chim. Acta* **2008**, *620 (1–2)*, 8–26.

(4) Sailor, M. J. *ACS Nano* **2007**, *1 (4)*, 248–252.

(5) Jane, A.; Dronov, R.; Hodges, A.; Voelcker, N. H. *Trends Biotechnol.* **2009**, *27 (4)*, 230–239.

(6) Kilian, K.; Böcking, T.; Gooding, J. J. *Chem. Commun. (Camb)*. **2009**, *6*, 630–640.

(7) Dhanekar, S.; Jain, S. *Biosens. Bioelectron.* **2013**, *41*, 54–64.

(8) Sailor, M. J. Porous Silicon in Practice: Preparation, Characterization and Applications; Wiley-VCH: Weinheim, Germany, 2011.

(9) Lin, V. S.-Y.; Motesharei, K.; Dancil, K.-P. S.; Sailor, M. J.; Ghadiri, M. R. *Science* **1997**, *278(5339)*, 840–843.

(10) Francia, G. Di; Ferrara, V. La; Manzo, S.; Chiavarini, S. *Biosens. Bioelectron*. ***2005***, *21 (4)*, 661–665.

(11) De Stefano, L.; Arcari, P.; Lamberti, A.; Sanges, C.; Rotiroti, L.; Rea, I.; Rendina, I. *Sensors* **2007**, *7 (2)*, 214–221.

(12) Dancil, K. S.; Greiner, D. P.; Sailor, M. J. 1999, *J. Am. Chem. Soc.14*, 7925–7930.

(13) Schwartz, M. P.; Alvarez, S. D.; Sailor, M. J. **2007**, *J. Am. Chem. Soc. 79 (1)*, 327–334.

(14) Pacholski, C.; Yu, C.; Miskelly, G. M.; Godin, D.; Sailor, M. J. J. Am. Chem. Soc. 2006, *128 (13)*, 4250–4252.

(15) Bonanno, L. M.; DeLouise, L. *Biosens. Bioelectron*. **2007**, 23 (3), 444–448.

(16) Janshoff, A.; Dancil, K. S.; Steinem, C.; Greiner, D. P.; Lin, V. S.; Gurtner, C.; Motesharei, K.; Sailor, M. J.; Ghadiri, M. R., *J. Am. Chem. Soc.* **1998,** *18*, 12108–12116

(17) Estephan, E.; Saab, M.-B.; Agarwal, V.; Cuisinier, F. J. G.; Larroque, C.; Gergely, C. *Adv. Funct. Mater.* **2011**, *21 (11)*, 2003–2011.

(18) Urmann, K.; Walter, J.-G.; Scheper, T.; Segal, E. *Anal. Chem.* **2015**, *87 (3)*, 1999–2006.

(19) Kilian, K. a.; Bocking, T.; Gaus, K.; King-Lacroix, J.; Gal, M.; Gooding, J. J. *Chem. Commun.* **2007**, *19*, 1936.

(20) De Stefano, L.; Rotiroti, L.; Rendina, I.; Moretti, L.; Scognamiglio, V.; Rossi, M.; D'Auria, S. *Biosens. Bioelectron.* **2006**, *21 (8)*, 1664–1667.

(21) Bonanno, L. M.; Delouise, L. A. *Anal.Chem.* **2010**, *82 (2)*, 714–722.

(22) Bonanno, L. M.; Kwong, T. C.; DeLouise, L. A. *Anal. Chem.* **2010**, *82 (23)*, 9711–9718.

(23) Krismastuti, F. S. H.; Brooks, W. L. A.; Sweetman, M. J.; Sumerlin, B. S.; Voelcker, N. H. *J. Mater. Chem. B* **2014**, *2 (25)*, 3972.

(24) Sohn, H.; Le, S.; Sailor, M. J.; Trogler, W. C. *J. Am. Chem. Soc.* **2000**, *17*, 5399–5400.

(25) Kilian, K. A.; Böcking, T.; Gaus, K.; Gal, M.; Gooding, J. J.*ACS Nano* **2007**, 1 (4), 355–361.

(26) Orosco, M. M.; Pacholski, C.; Miskelly, G. M.; Sailor, M. J. *Adv. Mater.* **2006**, *18(11)*, 1393–1396.

(27) Orosco, M. M.; Pacholski, C.; Sailor, M. J. *Nat. Nanotechnol.* **2009**, *4 (4)*, 255–258.

(28) Shtenberg, G.; Massad-Ivanir, N.; Moscovitz, O.; Engin, S.; Sharon, M.; Fruk, L.; Segal, E. *Anal. Chem.* **2013**, *85 (3)*, 1951–1956.

(29) DeLouise, L. A; Kou, P. M.; Miller, B. L. *Anal. Chem.* **2005**, *77 (10)*, 3222–3230.

(30) Gupta, B.; Zhu, Y.; Guan, B.; Reece, P. J.; Gooding, J. J. *Analyst* **2013**, *138 (13)*, 3593–3615.

(31) Massad-Ivanir, N.; Shtenberg, G.; Tzur, A.; Krepker, M. A.; Segal, E. *Anal. Chem.* **2011**, *83 (9)*, 3282–3289.

(32) Tenenbaum, E.; Segal, E. Analyst. **2015**, *140 (22)*, 7726–7733.

(33) Vilensky, R.; Bercovici, M.; Segal, E. *Adv. Funct. Mater.* **2015**, *25(43)*, 6725-6732.

(34) Homola, J. Chem. Rev. 2008, 108 (2), 462–493.

(35) Szili, E. J.; Jane, A.; Low, S. P.; Sweetman, M.; Macardle, P.; Kumar, S.; Smart, R. S. C.; Voelcker, N. H. *Sensors Actuators B Chem*. **2011**, *160 (1)*, 341–348.

(36) Holthausen, D.; Vasani, R. B.; Mcinnes, S. J. P.; Ellis, A. V; Voelcker, N. H. ACS *Macro Lett.* **2012**,*1*, 919–921.

(37) Krismastuti, F. S. H.; Pace, S.; Voelcker, N. H. *Adv. Funct. Mater.* **2014**, *24 (23)*, 3639–3650.

(38) Gupta, B.; Mai, K.; Lowe, S. B.; Wakefield, D.; Di Girolamo, N.; Gaus, K.; Reece, P. J.; Gooding, J. J. *Anal. Chem.* **2015**, *87 (19)*, 9946–9953.

(39) Pacholski, C.; Sartor, M.; Sailor, M. J.; Cunin, F.; Miskelly, G. M. *J. Am. Chem. Soc.* **2005**, *127 (33)*, 11636–11645.

(40) Chen, M. Y.; Sailor, M. J. *Anal. Chem*. **2011**, *83 (18)*, 7186–7193.

(41) Schwarzenbach, H.; Hoon, D. S. B.; Pantel, K. *Nat. Rev. Cancer.* **2011**, *11 (6)*, 426 437.

(42) Ruminski, A. M.; Barillaro, G.; Chaffin, C.; Sailor, M. J. *Adv. Funct. Mater.* **2011**, *21 (8)*, 1511–1525.

(43) Putnam, F.W. The Plasma Proteins: Structure, Function and Genetic Control, 2nd ed., Frank W. Putnam, ed., *Vol. 1*, p. 141, 147, Academic Press, New York,1975.

(44) Pacholski, C. *Sensors (Basel).* **2013**, *13 (4)*, 4694–4713.

(45) Lasave, L. C.; Urteaga, R.; Koropecki, R. R.; Gonzalez, V. D.; Arce, R. D. *Colloids Surf. B. Biointerfaces*. **2013**, *111*, 354–359.

(46) Ellison, S. L. R.; Barwick, V. J.; Farrant, T. J. D. Practical Statistics for the Analytical Scientist: A Bench Guide; Ed. The Royal Society of Chemistry, UK, 2009; pp pp 155.

Figure captions

Fig. 1 SEM images, (a) cross-section and (b) top view, of a porous silicon (PS) layer. (c) Reflection spectra, recorded in air, of as made (black line) and oxidized (red line) PS. (d) Contact angles of deionized water (DIW) on as made and oxidized PS.

Fig. 2 (a) Reflection spectra of PS in acetate buffer before (black trace) and after injection of BSA 15 μM (red trace). (b-d) Interferograms of PS in acetate buffer (black trace) and after injection of BSA 15 μM (red trace) calculated over the spectral range 500-800 nm: (b) after differentiation of reflection spectra in (a); (c) after removal of the average value from (b); (d) after application of the absolute value function to (c).

Fig. 3 (a) Time-resolved IAW–IAW_0 value upon injection of BSA15 μM (acetate buffer pH = pI = 4.7) at a flow-rate of 25 μL/min: acetate buffer before injecting BSA (minutes 0-10), injection of BSA 15 μM (minutes 10-50), and acetate buffer after BSA injection (rinsing step, minutes 50-60). (b) Calibration curve IAW–IAW_0 *Vs* BSA concentration in semi-log scale (linear scale in inset) experimentally measured over 5 replicates, and best fitted (R^2= 0.989) with a sigmoidal function (red trace). The gray area underneath the calibration curve indicates IAW–IAW_0 values corresponding to BSA concentrations below the instrumental detection limit (20 pM, i.e. 20 femtomoles, 1 mL).

Figures

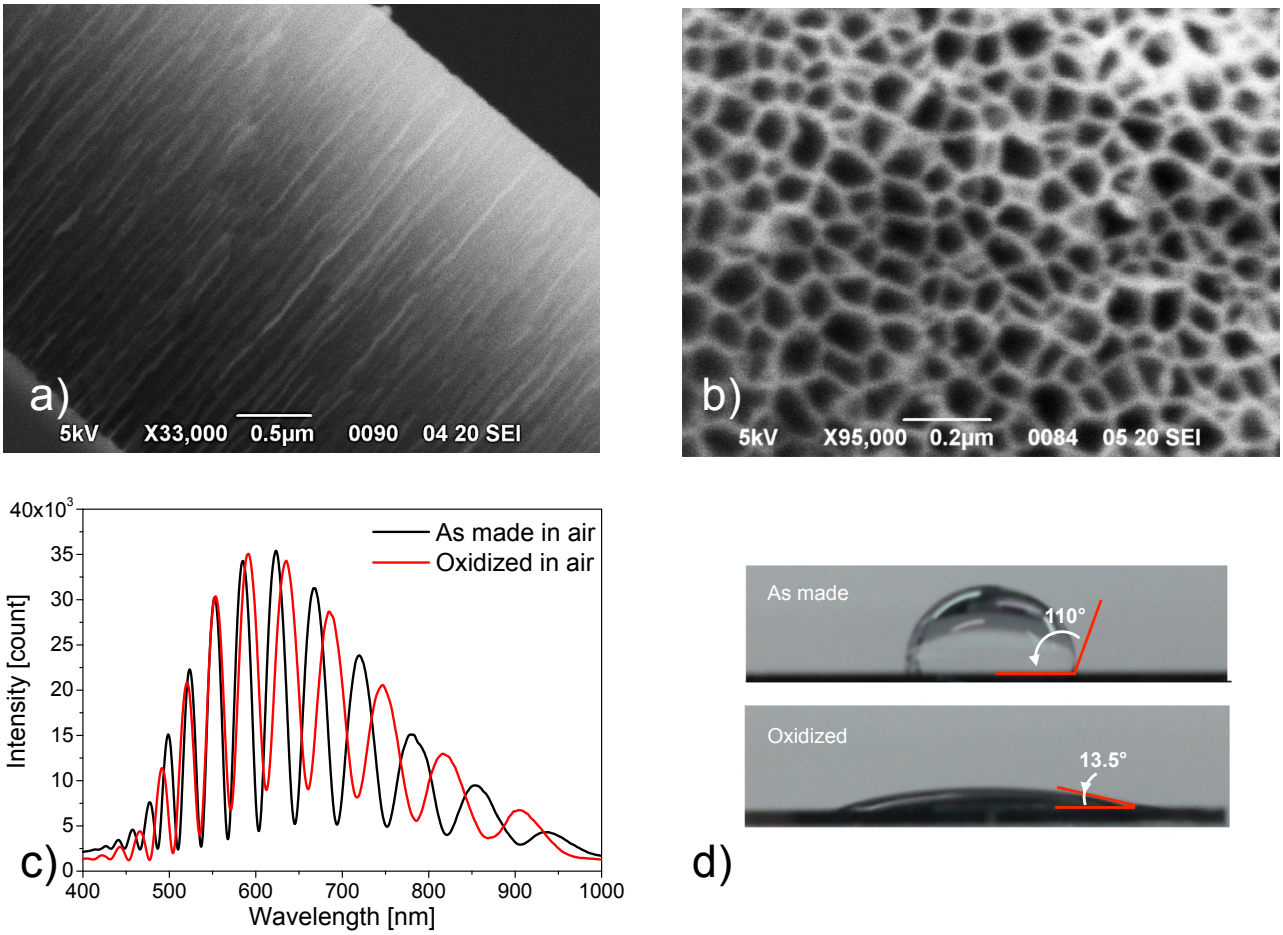

Figure 1

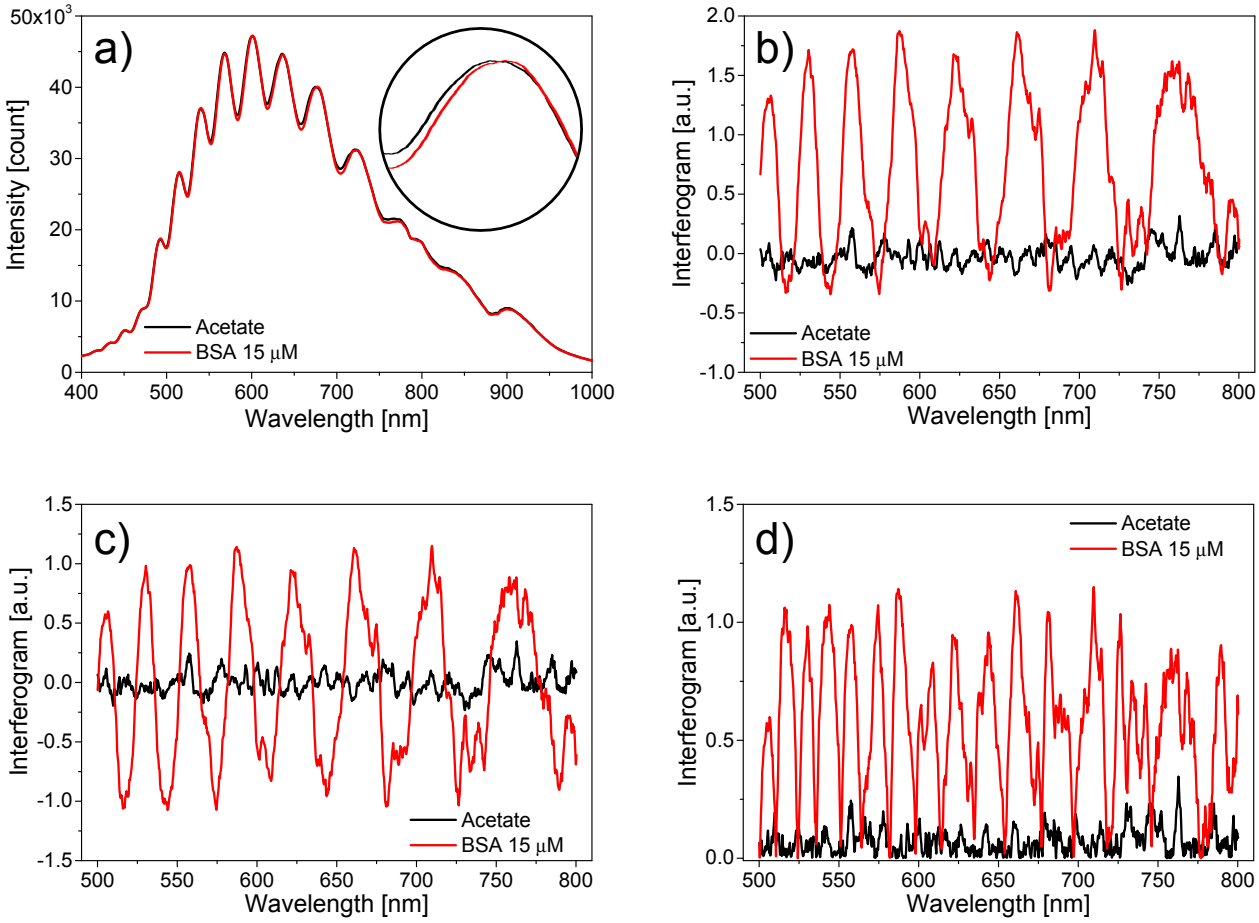
a)
50x10^3
Intensity [count]
Wavelength [nm]
Acetate
BSA 15 μM
b)
Interferogram [a.u.]
Wavelength [nm]
Acetate
BSA 15 μM
c)
Interferogram [a.u.]
Wavelength [nm]
Acetate
BSA 15 μM
d)
Interferogram [a.u.]
Wavelength [nm]
Acetate
BSA 15 μM

Figure 2

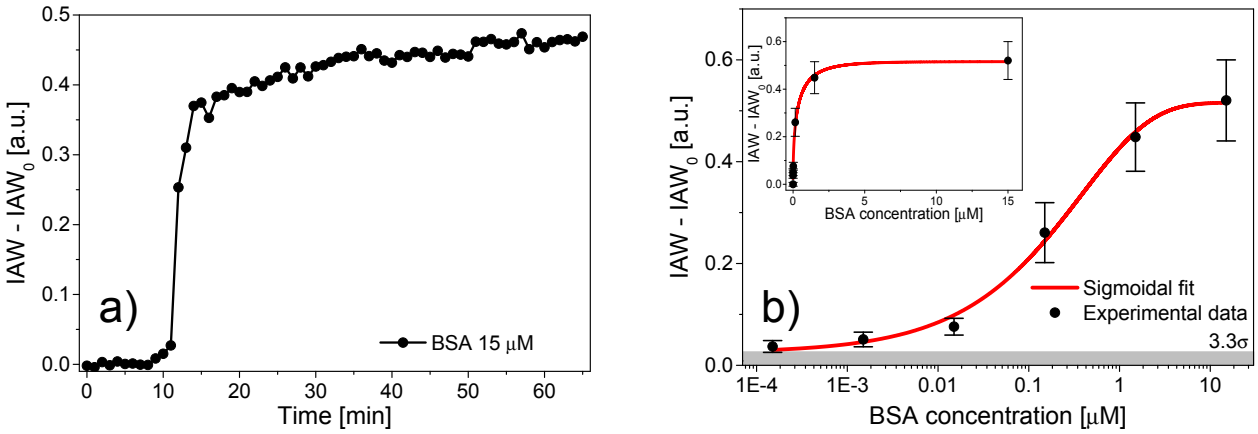
a)
BSA 15 μM
IAW - IAW0 [a.u.]
Time [min]
b)
Sigmoidal fit
Experimental data
3.3σ
BSA concentration [μM]

Figure3

For Table of Contents Only